



# A single phase photovoltaic inverter control for grid connected system

AUROBINDA PANDA\*, M K PATHAK and S P SRIVASTAVA

Department of Electrical Engineering, Indian Institute of Technology Roorkee, Roorkee,  
Uttarakhand 247667, India  
e-mail: aurobind.panda@gmail.com

MS received 15 October 2014; revised 2 June 2015; accepted 16 October 2015

**Abstract.** This paper presents a control scheme for single phase grid connected photovoltaic (PV) system operating under both grid connected and isolated grid mode. The control techniques include voltage and current control of grid-tie PV inverter. During grid connected mode, grid controls the amplitude and frequency of the PV inverter output voltage, and the inverter operates in a current controlled mode. The current controller for grid connected mode fulfills two requirements – namely, (i) during light load condition the excess energy generated from the PV inverter is fed to the grid and (ii) during an overload condition or in case of unfavorable atmospheric conditions the load demand is met by both PV inverter and the grid. In order to synchronize the PV inverter with the grid a dual transport delay based phase locked loop (PLL) is used. On the other hand, during isolated grid operation the PV inverter operates in voltage-controlled mode to maintain a constant amplitude and frequency of the voltage across the load. For the optimum use of the PV module, a modified P&O based maximum power point tracking (MPPT) controller is used which enables the maximum power extraction under varying irradiation and temperature conditions. The validity of the proposed system is verified through simulation as well as hardware implementation.

**Keywords.** Current controller; MPPT; photovoltaic; PLL; PV inverter; voltage controller.

## 1. Introduction

The principal source of electrical energy is the hydrocarbon based fossil fuel. CO<sub>2</sub> emission from fossil fuel based power plants is a major cause of global warming. In addition, the availability of such energy resources is very limited for the future consumption [1]. These are the reasons, which attract many researchers to work in the area of renewable energy. Among all the available renewable energy sources, solar photovoltaic (PV) system has several advantages such as clean energy and potential to provide sustainable electricity to remote areas [1, 2]. They can be installed in residential or commercial complexes to meet partial/full load demand. In case the power generated by PV system is more than the load demand, the excess power can be fed to the grid [3]. However, the major constraints in the development of a grid connected PV system are – cost of PV module and interfacing of PV inverter with the grid [4, 5]. Because of these challenges, it is necessary to use the energy of PV module optimally. Moreover, interfacing of PV system with the grid requires a number of controllers to handle many issues at the same time. Therefore, this paper presents all the controllers that are required for the development of a simpler form of grid connected PV system. Starting from the generation

side, an MPPT controller is used to maximize the utilization of solar power for a given insolation and temperature condition [6, 7]. In the instantaneous maximum power point (MPP) tracking (MPPT), the PV module is operated in conjunction with a DC–DC converter. Several MPPT schemes have been proposed in the literature [7]. Some of the popular MPPT schemes are perturbed and observe (P&O), incremental conductance (IC), open circuit voltage, short circuit current, etc. [7, 8]. The IC method is based on the fact that, the slope of the power curve is zero at MPP, negative on the right and positive on the left of the MPP. In [9], the author claims that this method is prone to failure in case of large change in atmospheric conditions. The fractional short circuit method of MPPT is discussed in [10]. However, as this method approximates a constant ratio, its accuracy cannot be guaranteed under varying weather conditions. To overcome the above-mentioned drawbacks, several artificial intelligence based MPPT controllers have been proposed [11, 12]. But these methods also have drawbacks such as, the requirement of large data storage and extensive computation. Among all the available MPPT techniques, the P&O is the most widely used MPPT scheme due to its simplicity. In [13], a review on P&O techniques has been presented. In this method the operating point oscillates around the MPP giving rise to wastage of energy. These oscillations can be minimized by reducing the fixed perturbation step size, but

\*For correspondence

then it takes more time to reach MPP. To overcome this conflicting situation, a modified P&O MPPT algorithm with variable step size is proposed. As the PV module output is a DC, power electronic devices are required to convert this DC power into AC power for grid interface [14], and for this DC–AC inverter is required. The synchronization of PV inverter with the grid is done with the help of a phase locked loop (PLL) [1, 15]. The main task of the PLL is to provide a unity power factor operation which includes synchronization of the inverter output current with the grid voltage [16–18]. There has been an increasing interest in PLL topologies for distributed generation system [14, 15]. It is a grid voltage phase detection structure which requires orthogonal voltages. In single-phase PLL, accurate and fast phase estimation can be obtained by processing a signal in phase with the grid voltage (original signal) and another one which is  $90^\circ$  phase shifted from it [19, 20]. The PLL, which generates orthogonal signals by delaying the original signal, is called a transport-delay PLL (TDPLL) [21]. This type of PLL is simple and its transient response is fast and smooth among all available PLL methods [22]. The other methods for generating orthogonal voltages are Hilbert transformation, Park transformation, etc. All these methods have shortcomings such as high complexity, nonlinearity and have slower response than TDPLL [23]. Artificial intelligence controller based PLL has also been proposed, however they are relatively more complex and are not suitable for control of PV inverters [24]. This paper presents a single-phase PLL structure, which generates the orthogonal signal by using transport delay. The main drawback of conventional TDPLL is its sensitivity to the grid frequency changes, since the delay is determined assuming constant frequency. Here, a modified TDPLL is suggested which uses two delay blocks

to make TDPLL robust against frequency variation. In addition to MPPT and grid synchronization controller, the other controllers required for a grid connected PV system are DC-link voltage controller, current controller and PV inverter voltage controller. Many research efforts have been going on in the area of grid interfaced PV system [25–27]. Current controllers are used to regulate the current, so that it follows the reference current, whereas voltage controller is used to control the PV inverter output voltage and frequency during isolated grid operation. There are several techniques to control the current and voltage such as PI controllers, hysteresis controllers, predictive controllers and sliding mode controllers. In [28], a hysteresis controller is proposed which is having fast response but operates at varying switching frequency. The predictive controller [29] overcomes the limitation of hysteresis controllers as it has constant switching frequency but it cannot properly match with change in atmospheric conditions. An analytical method is proposed in [30] to determine the control parameters in steady state, but this method cannot be implemented easily during transients, which are natural in PV systems. This paper uses PI controllers [31, 33] for both current and voltage control of the PV inverter system.

## 2. Grid connected rooftop photovoltaic system

Figure 1 shows the schematic diagram of a grid connected photovoltaic system. It includes two PV module, two DC–DC converters, inverter, controllers and the grid. The DC–DC converters along with an MPPT controller are used to extract the maximum power from each PV module. DC to AC converter is used to interface the PV system to the grid.

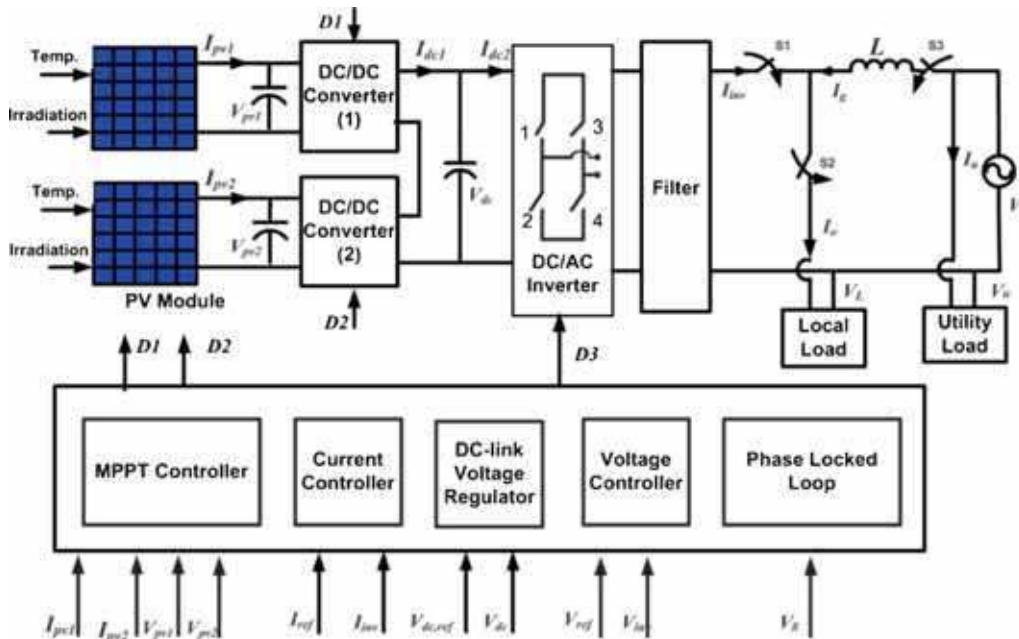
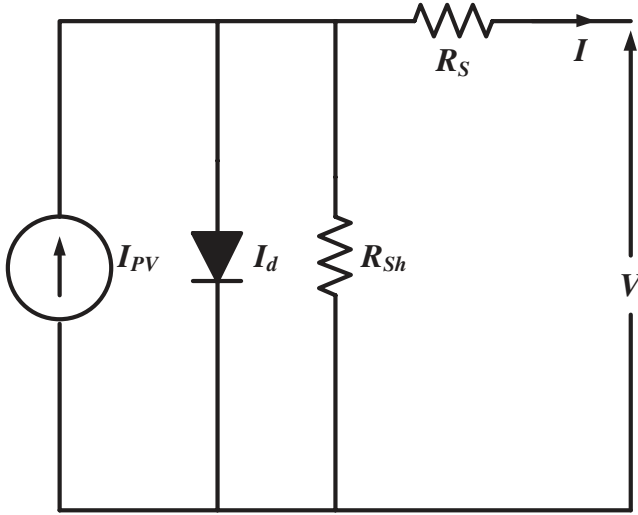


Figure 1. Schematic diagram of a 1- $\phi$  grid connected PV system [31].



**Figure 2.** Equivalent model of PV cell [32].

Phase locked loop (PLL) controller is used for the synchronization of PV inverter with the grid. During grid connected mode, inverter operates in a current controlled mode with the help of a current controller. While, in grid isolated mode, a voltage controller is used to maintain the required terminal voltage and frequency at a desired level.

### 3. PV modeling and parameter estimation

In order to analyze the grid connected PV system, it is essential to model the PV module connected to the system by using data available from the manufacturer's datasheet. However, some of the parameters required for the modeling of PV module are not given in the datasheet. All these parameters are estimated from datasheet values and then used in modeling. The equivalent circuit of a practical PV cell is shown in figure 2.

The characteristic equation of a PV cell is expressed as [4],

$$I = I_{PV} - I_0 \left[ \exp \left( \frac{V + IR_S}{N_s V_t} \right) - 1 \right] - \frac{V + IR_S}{R_{Sh}}. \quad (1)$$

The available parameters of the PV module and the parameters to be estimated are tabulated in table 1. The procedure for the parameter estimation is given below:

Since the exponential term in Eq. (1) is much larger than 1, it can be re-written as

$$I = I_{PV} - I_0 \left[ \exp \left( \frac{V + IR_S}{N_s V_t} \right) \right] - \frac{V + IR_S}{R_{Sh}}. \quad (2)$$

Substituting three significant-points of the  $I - V$  characteristic of PV module, namely: the short-circuit point (0,  $I_{SC}$ ), the maximum power point ( $V_{MPP}$ ,  $I_{MPP}$ ), and the open-circuit point ( $V_{OC}$ , 0) in Eq. (2) gives

$$I_{SC} = I_{PV} - I_0 \left[ \exp \left( \frac{I_{SC} R_S}{N_s V_t} \right) \right] - \frac{0 + I_{SC} R_S}{R_{Sh}} \quad (3)$$

$$I_{MPP} = I_{PV} - I_0 \left[ \exp \left( \frac{V_{MPP} + I_{MPP} R_S}{N_s V_t} \right) \right] - \frac{V_{MPP} + I_{MPP} R_S}{R_{Sh}} \quad (4)$$

$$I_{PV} = I_0 \left[ \exp \left( \frac{V_{OC}}{N_s V_t} \right) \right] + \frac{V_{OC}}{R_{Sh}}. \quad (5)$$

At MPP, the derivative of power with respect to voltage is zero [32].

$$\left. \frac{dP}{dV} \right|_{MPP} = 0. \quad (6)$$

Similarly, at short circuit condition [32],

$$\left. \frac{dI}{dV} \right|_{I=I_{SC}} = -\frac{1}{R_{Sh}}. \quad (7)$$

From Eqs. (5) and (3),  $I_0$  can be expressed as

$$I_0 = \left( I_{SC} - \frac{V_{OC} - I_{SC} R_S}{R_{Sh}} \right) \exp \left( \frac{-V_{OC}}{N_s V_t} \right). \quad (8)$$

Substituting Eq. (8) in Eq. (5)

$$I_{PV} = I_{SC} + \frac{I_{SC} R_S}{R_{Sh}} \quad (9)$$

From Eq. (4) and Eq. (9),

$$I_{MPP} = \left[ I_{SC} - \frac{V_{MPP} + I_{MPP} R_S - I_{SC} R_S}{R_{Sh}} \right] - \left[ \left( I_{SC} - \frac{V_{OC} - I_{SC} R_S}{R_{Sh}} \right) e^{\left( \frac{V_{MPP} + I_{MPP} R_S - V_{OC}}{N_s V_t} \right)} \right]. \quad (10)$$

The transcendental equation (10) still contains three unknown parameters:  $R_S$ ,  $R_{Sh}$  and  $V_t$ . Therefore, for the estimation of all these parameters additional equations are required which are derived below.

The rate of change of power with respect to voltage at MPP can be written as

$$\left. \frac{dP}{dV} \right|_{MPP} = I_{MPP} + \frac{V_{MPP} \frac{\partial}{\partial V_{MPP}} f(V, I)}{1 - \frac{\partial}{\partial I_{MPP}} f(V, I)}. \quad (11)$$

**Table 1.** Available and estimated PV module parameters.

Parameters available in datasheet at STCs <sup>a</sup>	Parameters to be estimated
$I_{MPP}$ , $V_{MPP}$ , $K_I$ , $K_V$ , $P_{MAX,e}$ , $V_{OC}$ and $I_{SC}$	$a$ , $R_S$ , $R_{Sh}$ , $I_{PV}$ and $I_0$

<sup>a</sup>Standard test conditions (STCs) of temperature (25°C) and solar irradiation (1000 W/m<sup>2</sup>).

where

$$\frac{\partial f(V, I)}{\partial V_{MPP}} = \frac{(V_{OC} - I_{SC}(R_S + R_{Sh})) \exp\left(\frac{V_{MPP} + I_{MPP}R_S - V_{OC}}{N_s V_t}\right)}{N_s V_t R_{Sh}} - \frac{1}{R_{Sh}} \quad (12)$$

$$\frac{\partial f(V, I)}{\partial I_{MPP}} = \frac{(V_{OC} - I_{SC}(R_S + R_{Sh})) \exp\left(\frac{V_{MPP} + I_{MPP}R_S - V_{OC}}{N_s V_t}\right)}{N_s V_t R_{Sh}} R_S - \frac{R_S}{R_{Sh}}. \quad (13)$$

By substituting Eq. (12) and Eq. (13) in Eq. (11), we have

$$\frac{dP}{dV}\bigg|_{MPP} = I_{MPP} + V_{MPP} \frac{\frac{(V_{OC} - I_{SC}(R_S + R_{Sh})) \exp\left(\frac{V_{MPP} + I_{MPP}R_S - V_{OC}}{N_s V_t}\right)}{N_s V_t R_{Sh}} - \frac{1}{R_{Sh}}}{1 + \frac{I R_S (I_{SC}(R_S + R_{Sh}) - V_{OC}) \exp\left(\frac{V_{MPP} + I_{MPP}R_S - V_{OC}}{N_s V_t}\right)}{N_s V_t R_{Sh}}} + \frac{R_S}{R_{Sh}} = 0. \quad (14)$$

Similarly, substituting Eq. (12) and Eq. (13) in Eq. (7), we have

$$\frac{dI}{dV}\bigg|_{(0, I_{SC})} = -\frac{1}{R_{Sh}} = \frac{\frac{I(V_{OC} - I_{SC}(R_S + R_{Sh})) \exp\left(\frac{I_{SC}R_S - V_{OC}}{N_s V_t}\right)}{N_s V_t R_{Sh}} - \frac{1}{R_{Sh}}}{1 + \frac{(I_{SC}(R_S + R_{Sh}) - V_{OC}) \exp\left(\frac{I_{SC}R_S - V_{OC}}{N_s V_t}\right)}{N_s V_t R_{Sh}}} + \frac{R_S}{R_{Sh}}. \quad (15)$$

Finally, five Eqs. (8), (9), (10), (14) and (15) are to be solved to calculate five unknown parameters. It is seen that, (10), (14) and (15) are transcendental in nature. Further, these three equations are completely independent of  $I_{PV}$  and  $I_0$  hence, the numerical method problem reduces to the determination of three unknowns from three equations:  $V_t$ ,  $R_S$  and  $R_{Sh}$ , which can be solved by using Gauss–Seidel method and then these values are used to obtain the value of  $I_0$  and then  $I_{PV}$  from Eq. (8) and (9) respectively. A case study to find the parameters of the PV module using above equations is carried out while using a PV module from the manufacturer, Maharishi Solar, India (<http://www.maharishisolar.com/>),. The values provided on the datasheet are tabulated in table 2 and are followed by the values of the estimated parameters.

#### 4. Control strategy

Following controllers are used for the development of a single-phase grid connected PV system:

- (1) Maximum power point tracking controller
- (2) Grid synchronization controller
- (3) PV inverter controller

The detailed description on each controller is given one by one in the following subsections:

##### 4.1 Maximum power point tracking control

A DC–DC converter (step up/ step down) serves the purpose of extracting maximum power from the PV module. By

**Table 2.** Datasheet's and estimated parameters of PV module.

Available datasheet parameters of PV module (ProductId.120 H24, Maharishi Solar, India)						
$I_{SC}$	$V_{OC}$	$V_{MPP}$	$I_{MPP}$	$P_{MPP}$	$K_V$	$K_I$
3.82 A	44.11 V	35.62 V	3.595 A	128.1 W	−2.10 mV/cell/° c	15 μ A/cell/° c
Estimated parameters						
$I_{PV}$	$I_0$	$R_S$	$R_{Sh}$	$A$		
3.82 A	0.102 μ A	0.31 Ω	600 Ω	1.2		

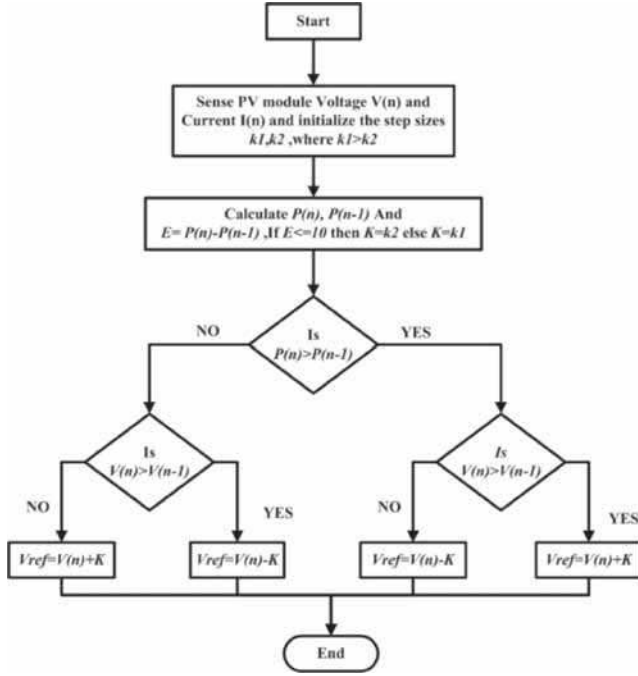


**Figure 3.** Flow chart for the MPPT control of PV module.

changing the duty cycle the load impedance as seen by the source is varied and matched at the point of the peak power with the source [6]. The perturb and observe (P&O) method is used here. It is an iterative method for obtaining MPP. It measures the PV array characteristics, and then perturbs the operating point of PV module to obtain the change in direction. The maximum point is reached when the rate of change of power with respect to voltage is zero. However, the major drawback of the conventional P&O is that, the process is repeated periodically until the MPP is reached. The system then oscillates about the MPP. The oscillation can be minimized by reducing the perturbation step size. However, a smaller perturbation size slows down the MPPT. An improved P&O algorithm is used here as a solution to this conflicting problem, which is shown in figure 3. Here, instead of the same perturbation size throughout the process, two step sizes ( $k1$  and  $k2$ ,  $k1 > k2$ ) are used. The operating voltage of the PV module is perturbed and the resulting change in power is measured. If  $dP/dV$  is positive, the perturbation of the operating voltage should be in the same direction as the increment. However, if it is negative, the system operating point is moving away from MPPT and the operating voltage should be perturbed in the opposite direction. Initially, when the error, i.e.  $E = P(n) - P(n-1)$  is large the algorithm selects the step size as  $K = k1$  to have a fast tracking of MPP. However, at the instant when  $E \leq 10W$  i.e. less than 8% of the maximum power, a step size of  $k2$  is chosen to have a minimum oscillation at the MPP. The exact value of  $k1$  is chosen based on the tracking time of MPP and it can be calculated as follows

Let,  $T$  = Maximum tracking time of MPPT controller and  $T_s$  = Sampling time of the controller. Number of samples

(or iteration) required for the MPPT controller to reach the MPP,  $N_s = T/T_s$ . In worst possible condition, the operating point has to cover from 0 V to  $V_{MPP}$  V (under STCs) within this  $N_s$  iteration. Therefore  $k1$  can be calculated as,  $k1 = V_{MPP} / N_s$ .

However, to minimize the power ripple at MPP, the step size  $k2$  is chosen as 1/10 times of  $k1$

#### 4.2 Grid synchronization controller

Synchronization between the PV inverter and the grid means that both will have the same phase angle, frequency and amplitude. In order to accomplish this, a 1- $\phi$  phase locked loop (PLL) is used. It is a feedback control system which automatically adjusts the phase of a locally generated signal to match the phase of an input signal and hence provide a unity power factor operation. In a grid connected PV system the objective of the PLL is to synchronize the inverter output current with the grid voltage. The schematic diagram of the 1- $\phi$  PLL is shown in figure 4. Here the input to the PLL structure is the grid voltage and output is its phase angle. This phase angle is used to generate the sine wave which acts as a reference signal to the control system. The time required for the synchronization is dependent on the PI block parameters, which are computed below.

From the schematic diagram it can be observed that the error in the PI controller of the PLL structure is given by

$$e = V_g \sin \theta_g \cos \theta - V_g \cos \theta_g \sin \theta = V_g \sin(\theta_g - \theta), \quad (16)$$

where  $\theta_g$  and  $\theta$  are phase angles of the grid and the PLL respectively.

In order to tune the parameters of PI controller, the input to the PI controller is linearized around a working point. Under steady state operation, the error in PI controller is zero and the linearized error in PI controller can be expressed by Taylor series as

$$f(x) \approx f(x_0) + f'(x_0) \cdot (x - x_0) \Leftrightarrow \sin(x)|_{x=0} = \cos(0)(x - 0) = x. \quad (17)$$

Thus, the error in PI controller becomes

$$\varepsilon = V_g(\theta_g - \theta). \quad (18)$$

The linearized small signal transfer function of the PLL is given by

$$\begin{aligned} PLL(s) &= \frac{V_g \left( K_P + \frac{K_I}{s} \right) \frac{1}{s}}{1 + V_g \left( K_P + \frac{K_I}{s} \right) \frac{1}{s}} \\ &= \frac{V_g \left( \frac{K_P}{K_I} \right) (1 + s K_I)}{s^2 + V_g K_P s + V_g \left( \frac{K_P}{K_I} \right)}. \end{aligned} \quad (19)$$

This is a second order system with one real zero.  $K_p$  is the proportional gain and  $K_I$  is the integral gain. The natural frequency and damping ratio can thus be stated as  $\omega_n =$

$\sqrt{\frac{V_g K_P}{K_I}}$  and  $\xi = \sqrt{\frac{V_g K_P K_I}{4}}$  respectively. The relationship between the natural frequency and the rise time for a second order system is known to be  $t_r \approx \frac{1.8}{\omega_n}$  [34]. The parameters describing the PI controller can then be specified in terms of rise time and grid voltage amplitude,  $K_I \approx \frac{\sqrt{2}}{\omega_n} \approx 0.79 t_r$  and  $K_P \approx \frac{\omega_n \sqrt{2}}{\hat{V}_g} \approx \frac{2.55}{t_r \hat{V}_g}$ . For a rise time of 5 ms, with optimal damping the parameters of the PI controller equals,  $K_P = 12.75$  and  $K_I = 3.95 \times 10^{-3}$ .

However, if the grid frequency differs from the nominal 50 Hz, the output from the 5 ms delay block in figure 4 is  $\cos(\theta_g) + A \sin(\theta_g)$ . Assuming that a cosine trigonometric function is used to compute the  $\cos(\theta)$ , the error into the PI controller becomes

$$Err = V_g \sin(\theta_g - \theta) - V_g A \sin(\theta_g) \cdot \sin(\theta) \quad (20)$$

Which contains an additional AC component at  $(\omega_g + \omega)$  rad/sec, which would lead to an error in PLL output, which is the major drawback of the conventional transport delay based PLL. A modified PLL is developed to cancel out errors because of input frequency variation. In modified PLL, the cosine of the PLL in feedback path is replaced by a sine function with another 5 ms delay block. With this dual

transport delay based PLL (DTDPLL), the error into the PI controller becomes

$$\begin{aligned} Err &= V_g \sin(\theta_g) [\cos(\theta) + A \sin(\theta)] \\ &\quad - V_g [\cos(\theta_g) + A \sin(\theta_g)] \cdot \sin(\theta) \\ &= V_g \sin(\theta_g - \theta). \end{aligned} \quad (21)$$

From Eq. (21), it is observed that the error due to input frequency variation is cancelled out by feedback transport delay block. This has been validated by simulation results, which is given in section 6.

### 4.3 PV inverter controller

Since the PV system is operated in both grid connected and grid isolated mode, the controller requirement of which are different and hence discussed separately in the following subsections.

**4.3a Grid connected mode:** During grid connected mode, the PV inverter operates as a current controlled source to generate an output current based on reference current [35, 36]. The regulation of DC-link voltage carries the information regarding the exchange of active power between PV module and grid. Thus the output of DC-link controller results

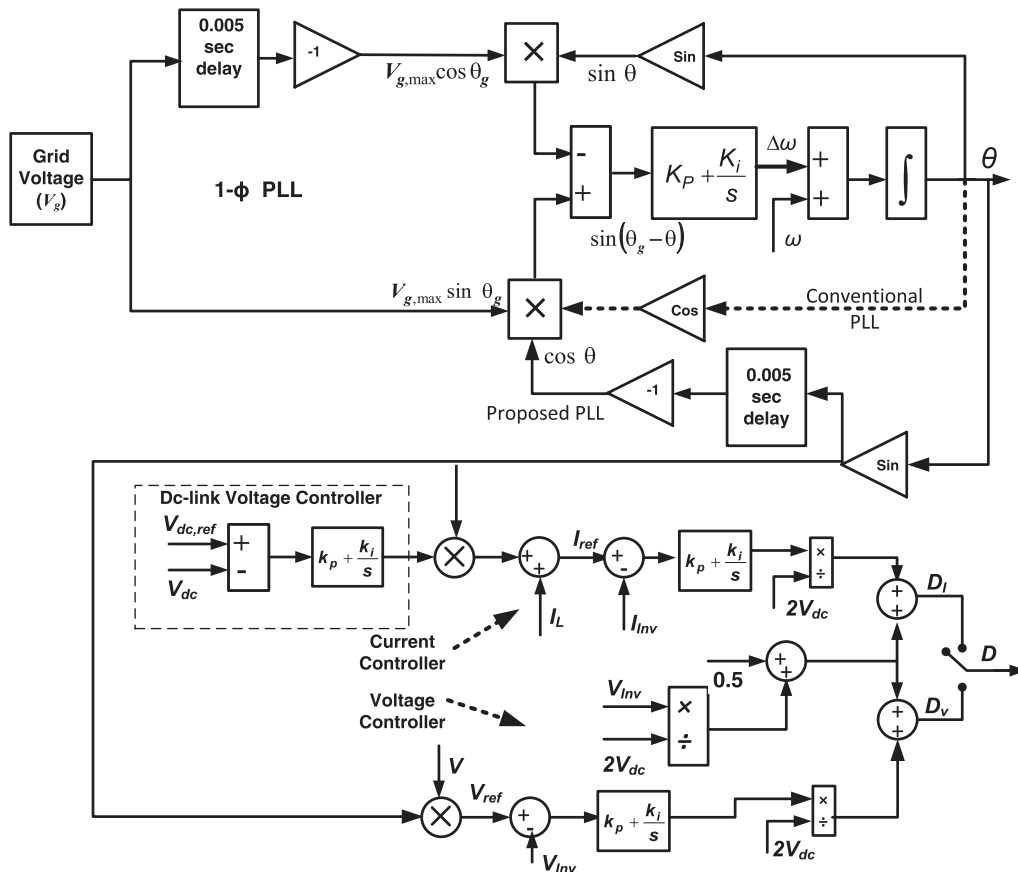


**Figure 4.** Complete control circuit for the proposed system.

in an active current. The block diagram of DC-link voltage controller for 1- $\phi$  two-level PV inverter is given in figure 4. Here the actual DC-link voltage of PV inverter ( $v_{dc}$ ) is sensed and passed through a first-order low pass filter (LPF) to eliminate the switching ripples. The difference of this filtered DC-link voltage and reference DC-link voltage ( $v_{dc}^*$ ) is given to a PI controller to regulate the DC-link voltage.

The DC-link voltage error ( $\Delta v_{err}$ ) in  $n^{th}$  sampling instant is given as

$$\Delta v_{err}(n) = v_{dc}^*(n) - v_{dc}(n). \quad (22)$$

The output of the PI controller at  $n^{th}$  sampling instant is expressed as

$$i_{inv}^*(n) = i_{inv}^*(n-1) + K_{P1}(\Delta v_{err}(n) - \Delta v_{err}(n-1)) + K_{I1}\Delta v_{err}(n). \quad (23)$$

where  $K_{P1}$  and  $K_{I1}$  are proportional and integral gains of the DC-link voltage controller.

The output of the DC-link voltage controller gives the peak value of the active current which is multiplied with the grid voltage template to generate the reference current for the PV inverter. With this control, the PV inverter can feed the local load with a maximum current up to reference current. If the load requirement is more than the PV generation, then the extra current is extracted from the grid. Similarly, when the load requirement is less than the PV generation, then the surplus power is fed to the grid. These two modes of operation are given in figure 5(a) and figure 5(b) respectively.

In this mode, the actual inverter current is compared with the reference current. The error is then fed to a PI controller. The output of the PI controller generates a change in the duty ratio ( $\hat{d}$ ) which is added to the steady state value of the duty ratio (D) to generate a modulating signal. The complete mathematical equation for the development of the modulating signal is explained below.

For a two level inverter as shown in figure 1, when switch '1' and '4' are ON, the output voltage  $V_0 = V_{dc}$  and when '2' and '3' are ON,  $V_0 = -V_{dc}$ . Therefore, the volt-second balance equation for the two level inverter can be written as

$$V_0 T = V_{dc}DT + (-V_{dc})(1-D)T = 2V_{dc}DT - V_{dc}T. \quad (24)$$

Under steady state the duty cycle of a two level inverter can be represented as

$$D = 0.5 + \frac{V_0}{2V_{dc}}. \quad (25)$$

For the closed loop control under grid connected mode,  $V_0$  can be replaced by  $V_{inv}$  and hence the duty cycle can be written as

$$D = 0.5 + \frac{V_{inv}}{2V_{dc}}. \quad (26)$$

The generated modulating signal during grid connected mode can be written as

$$m = \underbrace{\left(0.5 + \frac{V_{inv}}{2V_{dc}}\right)}_D + \underbrace{\frac{\left(K_P + \frac{K_I}{s}\right)(I_{ref} - I_{Inv})}{2V_{dc}}}_{\hat{d}}. \quad (27)$$

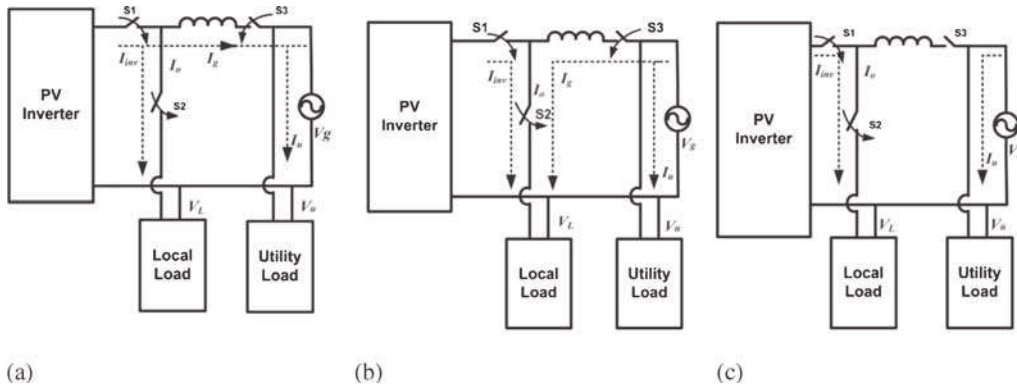


**Figure 5.** (a) During light load condition; (b) during overload condition; (c) during isolated grid operation.

**Table 3.** Specification of components for hardware development.

Items	Specification and features
Switches	Power MOSFET, IRFP460 ( <a href="http://www.st.com/web/en/resource/technical/document/datasheet/CD00001584.pdf">http://www.st.com/web/en/resource/technical/document/datasheet/CD00001584.pdf</a> )
Isolation amplifier	AD202JY (analog devices) ( <a href="http://www.analog.com/en/search.html?q=ad202jy">http://www.analog.com/en/search.html?q=ad202jy</a> )
Current sensor	TELCON HTP 50 ( <a href="http://www.telcon.co.uk/PDF%20Files/HTP25.pdf">http://www.telcon.co.uk/PDF%20Files/HTP25.pdf</a> )
dSPACE board	DS1104 (dynafusion)
Solar power meter	TM-207
Buck converter	Inductor: 2 mH , capacitor: 550 $\mu$ F
Filter	L: 0.2 mH, C: 100 $\mu$ F
Grid	40 V (peak), 50 Hz supply grid side Inductor value: 0.05 mH

Finally, the modulating signal is compared with a 3 kHz triangular carrier signal to generate the required switching pulses for the PV inverter to generate an inverter current, which is equal to the reference current.

**4.3b Grid isolation mode:** During grid isolation mode, the PV inverter operates as a voltage controlled source to generate an output voltage based on reference voltage. Similar to current controller mode, PLL is used to find the phase angle of the grid voltage. The phase angle generated by the PLL along with the amplitude is used to generate the reference voltage. Although inverter is operating in isolated mode, the PLL is necessary to ensure that whenever the grid is reconnected, the inverter voltage is synchronized with it. In isolated grid operation, the actual inverter output voltage is compared with the reference voltage. The error is then fed to a PI controller. The output of the PI controller generates a change in the duty ratio ( $\hat{d}$ ) which is then added to the steady state value of the duty ratio ( $D$ ) to generate the

modulating signal. The complete mathematical equation for the development of the modulating signal in voltage-controlled mode is given in the following equation.

$$m = \underbrace{\left(0.5 + \frac{V_{inv}}{2V_{dc}}\right)}_D + \underbrace{\frac{\left(K_P + \frac{K_L}{s}\right)(V_{ref} - V_{Inv})}{2V_{dc}}}_{\hat{d}}. \quad (28)$$

Finally, the modulating signal is compared with a 3 kHz triangular carrier signal to generate the required switching pulses for the inverter. The control circuit and power flow operation under this mode are shown in figure 4 and figure 5(c) respectively.

## 5. System hardware development

A prototype laboratory model for a single phase grid connected PV system is developed using specifications tabulated in table 3 and is shown in figure 6. Various system parameters



Figure 6. Laboratory prototype model of PVDG system.

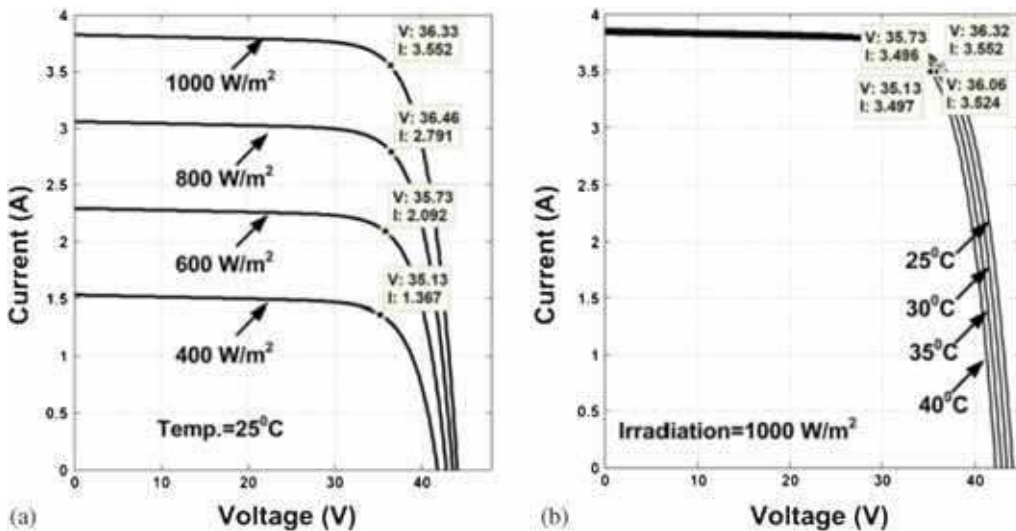
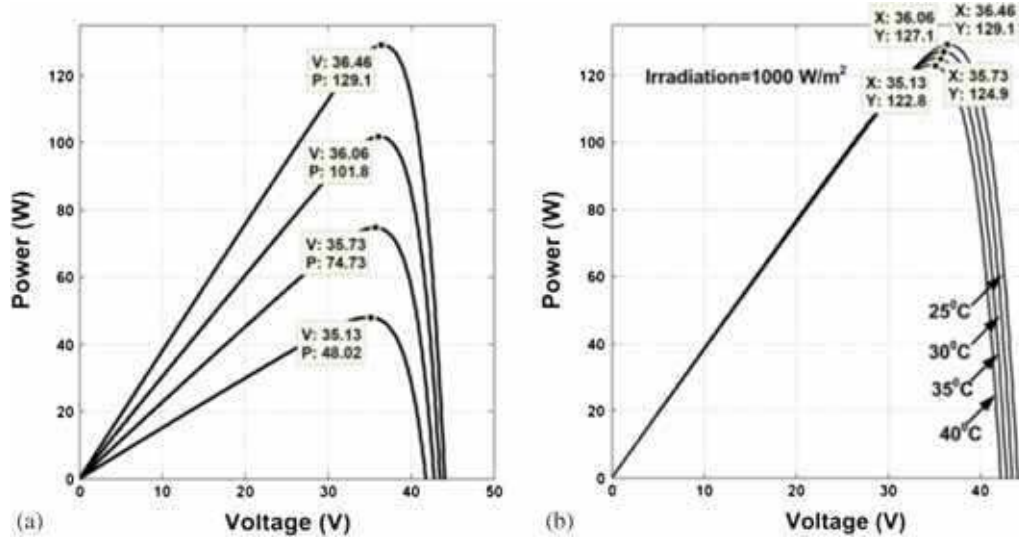
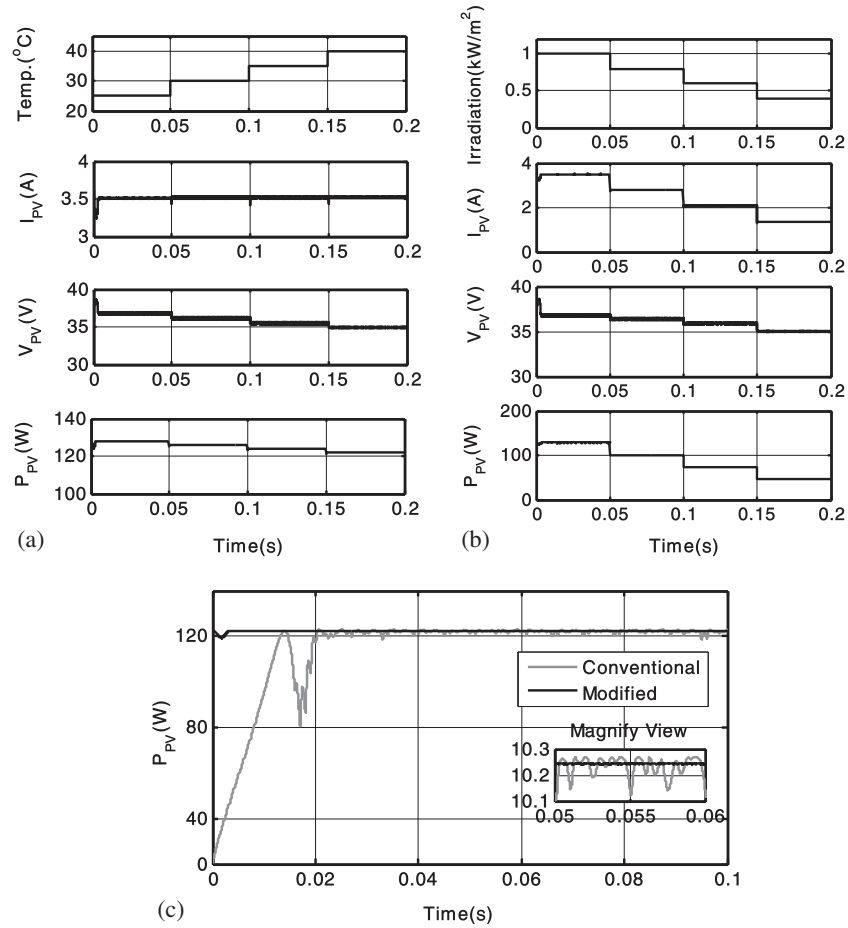


Figure 7. Simulation results of current vs. voltage characteristics of PV module. (a) Influenced by insolation but at constant temperature; (b) influenced by temperature but at constant insolation.



**Figure 8.** Simulation results of power vs. voltage characteristics of PV module. (a) Influenced by insolation but at constant temperature; (b) influenced by temperature but at constant Insolation.



**Figure 9.** Simulation results of maximum power point tracking of PV module (a) at varying temperature; (b) varying irradiation condition; (c) comparative analysis of conventional and modified MPPT.

like voltage and current are measured and conditioned using Hall-effect current sensors (TELCON HTP 50) and isolation amplifiers (AD202JY). The control algorithm is first developed in the MATLAB Simulink environment and the real time workshop of MATLAB generates the optimized C-code for real time implementation. The interface between MATLAB and Digital signal processor (DSP, DS1104 of dSPACE) allows the control algorithm to be run on the hardware, which is an MPC8240 processor. Switching signals obtained from the controller are given to the power MOSFETs after proper isolation and amplification. For the testing of the complete prototype, the outputs of the DC–DC converters are fed to a two-level inverter whose output is connected to a resistive type local load. For the validation of grid interfacing, a 40V (peak) (or 28.28 V (RMS)), 50 Hz grid is prepared in the laboratory with the help of an isolation and step down transformer.

## 6. Results and discussion

### 6.1 Simulation results

In order to verify the performance of the aforementioned grid connected PV system, a computer-based simulation using MATLAB Simulink is carried out. For the validation purpose, two PV modules obtained from the manufacturer Maharishi Solar (<http://www.maharishisolar.com/>) are used. The manufacturer's datasheet of the PV Module is given in Appendix A. The simulation of the PV module is done under varying irradiation (400–1000 W/m<sup>2</sup>) and temperature (25°C to 40°C) conditions. The current vs. voltage characteristics and power vs. voltage characteristics for these conditions are shown in figure 7 and figure 8 respectively. At maximum power point, the simulation results of current, voltage and power under varying temperature and irradiation conditions are presented in figure 9(a) and figure 9(b) respectively. To show the comparative analysis between conventional P&O based MPPT and modified MPPT, a

simulation result is given in figure 9(c). It can be observed that the oscillation in the proposed MPPT scheme is less as compared to the conventional P&O method.

In order to validate the efficacy of DTDPLL for frequency other than 50 Hz input, the proposed PLL is simulated with an input frequency of 45 Hz. Initially the input signal is applied to the conventional PLL and after a few seconds, the i/p signal is fed to the proposed PLL. The corresponding simulation results are shown in figure 10. Figure 10(a) shows the output phase angle of the PLL in rad/s whereas figure 10(b) shows the i/p and o/p signal. It can be observed that, with conventional TDPLL the error is found to be significant when an input signal is having other than 50 Hz frequency. However, with proposed DTDPLL, the error is almost zero and input and output signals are found to be exactly in phase with each other. In order to show the dynamic performance of the proposed PLL under frequency variation, simulation results of input and output signals under different frequency inputs are shown in figure 11.

Finally, the single-phase grid connected PV system is simulated at STCs to observe both current and voltage control of PV Inverter. In grid connected mode, all the three switches

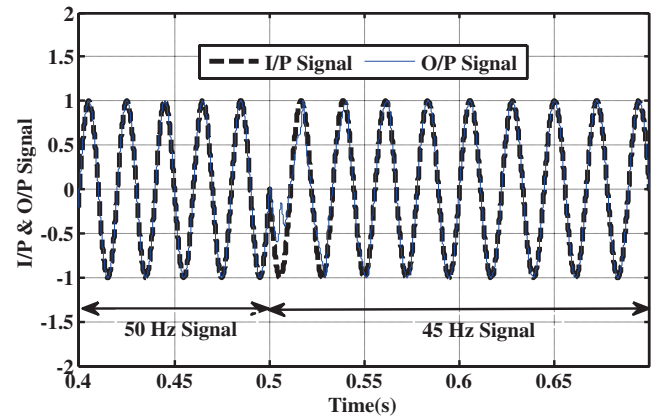


**Figure 11.** Input and output signal of proposed PLL with frequency variation.

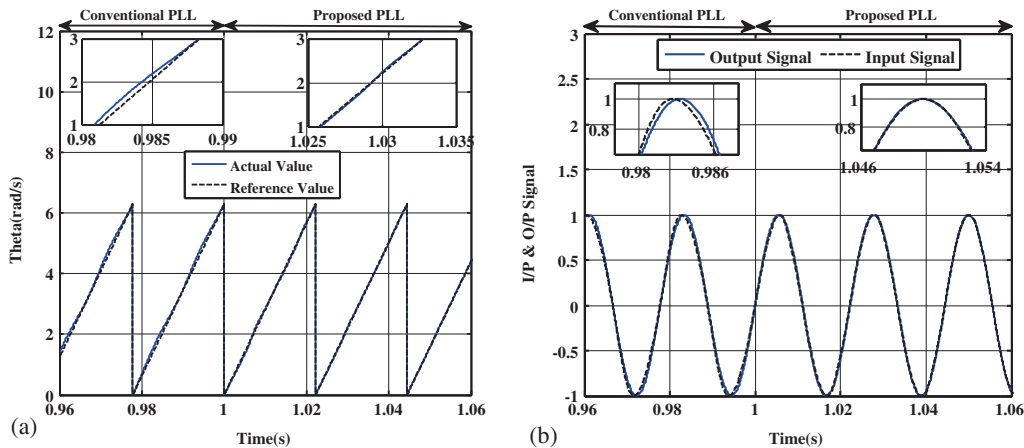


**Figure 10.** (a) Output phase angle; (b) input and output signal with conventional and proposed PLL when input signal frequency is of 45 Hz.

$S_1$ ,  $S_2$  and  $S_3$  are closed as shown in figure 5(a) and figure 5(b). Similarly, in isolated grid operation the switches  $S_1$ ,  $S_2$  are closed and  $S_3$  is open. During grid connected mode, the simulation results for both light load and overload conditions are given in figure 12. In this mode, the DC-link voltage controller generates the reference PV inverter current. The reference voltage for the DC-link voltage controller is set at 60 V and at STCs the reference current generated by the controller is 7.4 A (RMS). It is observed from the simulation results that, the PV inverter is able to generate the current equal to reference current. For light load condition, a resistive load of  $5\ \Omega$  is chosen, which demands an RMS current of 5.65 A. Therefore, the surplus PV power is fed to the grid. During this light load condition, the grid current is out of phase from PV inverter current and load current, which implies that the surplus current generated by the PV inverter

is fed to the grid. Similarly, for overload conditions, a resistive load of  $2\ \Omega$  is chosen. In this case, the load requirement is 14.14 A (RMS), which is more than the PV current (7.4 A), so the rest of the required load demand is met by the grid. It is observed from figure 12 that during overload condition the PV inverter current, load current and grid current are in the same phase, which means the load requirement is fulfilled by both PV inverter and the grid. During the transition period from light load to overload condition, the DC-link voltage changes from its reference value to compensate the increase in load current. This causes a drop in capacitor voltage, which is restored in 2–3 cycles. Similarly, during the transition period from an overload to light load condition, the drop in load current is responded by PV inverter with a rise in capacitor voltage, which is restored in 2–3 cycles to its reference value. The DC-link voltage controller

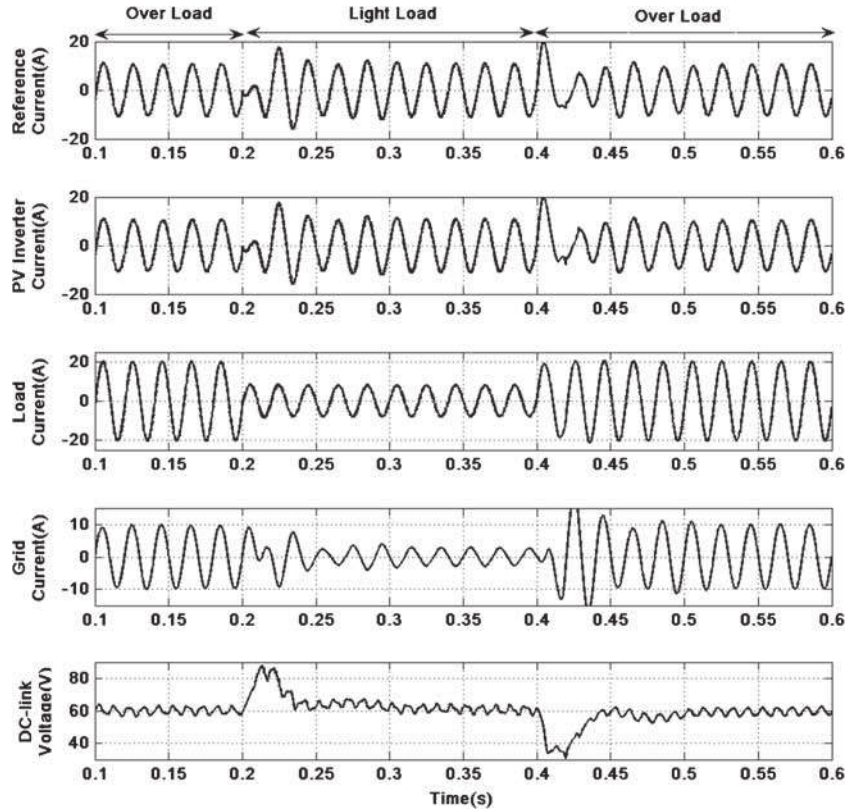


**Figure 12.** Simulation results during grid connected operation under both overload and light load condition.

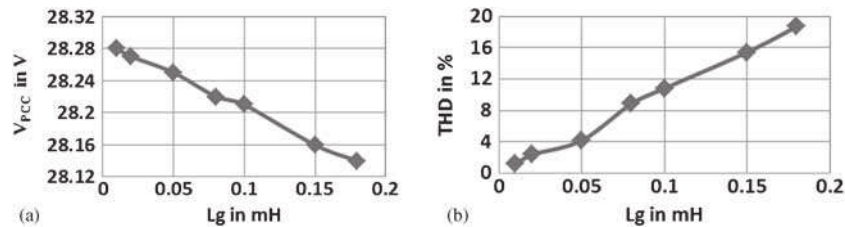


**Figure 13.** (a) Effect of grid inductor on the voltage at PCC; (b) THD of the grid voltage.

therefore, ensures the regulation of the capacitor voltage. The grid side inductor plays an important role during grid connected mode. It is designed based on high frequency current attenuation from the PV inverter to the grid. The high value of grid inductor effect significantly on the magnitude and %THD of voltage at PCC. This has been shown in graphical form in figure 13(a) and figure 13(b) respectively.

When the switch S3 is opened, the PV inverter switches to grid isolation mode to supply power to the local load. In this mode, the inverter is voltage controlled to maintain 40V (peak), 50 Hz. The voltage waveforms in this mode of operation are shown in figure 14. Initially the system is operated under grid-connected mode at  $t = 0.1$  s, the grid is isolated from the PV inverter. In this mode of operation, the PV inverter is operated in voltage-controlled mode to maintain a constant voltage across the load.

## 6.2 Experimental results

In the first part of the experimental validation the current vs. voltage and power vs. voltage characteristic of the PV module are plotted based on the experimental data and are shown in figure 15(a) and figure 15(b) respectively. For the validation of MPPT control, the developed DC–DC buck converter is tested on 26th June 2013 at 1:15 PM. The irradiation and temperature were measured as  $850 \text{ W/m}^2$  and  $35^\circ\text{C}$  respectively. A resistive load was connected across the converter and the obtained results are shown in figure 16(a). The experimental result shows the PV module output power, current and voltage. Initially, the MPPT controller was in enabled mode. The PV module output voltage; current and power are recorded as 32 V, 2.6 A and 83 W

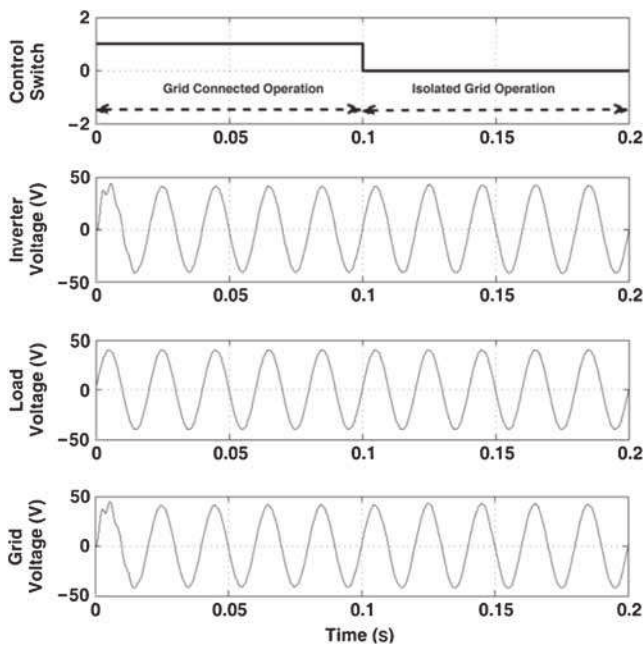


**Figure 14.** Simulation results during grid isolation mode.

respectively. After a few seconds, the MPPT controller is disabled. Under this condition, the PV module output voltage; current and power are recorded as 16 V, 2.6 A and 42 W respectively. Therefore, it is observed from figure 16(a) that with an MPPT controller the optimal power can be extracted from the PV module. In the second part of the experimental validation, the PV inverter is interfaced with the grid. For the interfacing purpose, a  $1 - \Phi$  PLL has been used. The output phase angle of the PLL is given in figure 16(b).

Finally, the experimental results of PV system are discussed for the following two modes of operation.

### Mode 1: Grid connected mode

In this mode the inverter is operated in light load and overload conditions to obtain both steady state and transient response.

#### (a) Light load condition

For the testing of prototype model under this mode, a  $5 \Omega$  resistive load is connected across the PV inverter. As explained in the previous section the inverter and load voltage under this mode are equal to the grid voltage, which is 28.28 V (rms) or 40 V (peak). The reference current generated by DC-link voltage controller during the test condition is 7.4 A (rms). The experimental results of PV inverter current, load current and grid current of the system under this mode are shown in figure 15(a). From this experimental result, it can be observed that under light load condition, the load requirement is less than the PV generation. Therefore the remaining PV inverter current is fed to the grid. It can also be observed from figure 15(a) that the inverter current, load current are in same phase, whereas the grid current is in opposite phase that demonstrates the surplus energy is fed to the grid. Under this mode of operation the harmonic spectrum of inverter current, load current and grid current are given in figure 16(i). The %THD for inverter current, load current and grid current are found out to be 4.1%, 3.9% and 3.3% respectively (figure 18(i)).

#### (b) Over load condition

For the testing of prototype model under this mode, a  $2 \Omega$  resistive load is connected across PV inverter, which acts as a local load. The experimental results of PV inverter current, load current and grid current of the system under current controlled mode are shown in figure 17(b). As the load requirement is more than the PV generation, the grid supplies the rest of the load current. It can also be observed from figure 17(b) that the inverter current, load current and grid current are in same phase, which means that load requirement is met by both PV Inverter and the grid. Under this mode of operation the harmonic spectrum of inverter current, load current and grid current are given in figure 16(ii). The THD for inverter current, load current and grid current are found out to be 4.1%, 3.4% and 2.3% respectively (figure 18(ii)).

## (c) Transient condition

The experimental results of PV inverter current, load current and grid current of the PV system during the transition period from overload to light load condition are shown in figure 17(c). It is observed that, during the transition

period from overload to light load condition, the drop in load current is responded by PV inverter with an increase in capacitor voltage which is restored back to its reference value (60V).

Finally, the comparison between simulation and experimental results during grid-connected mode is given in

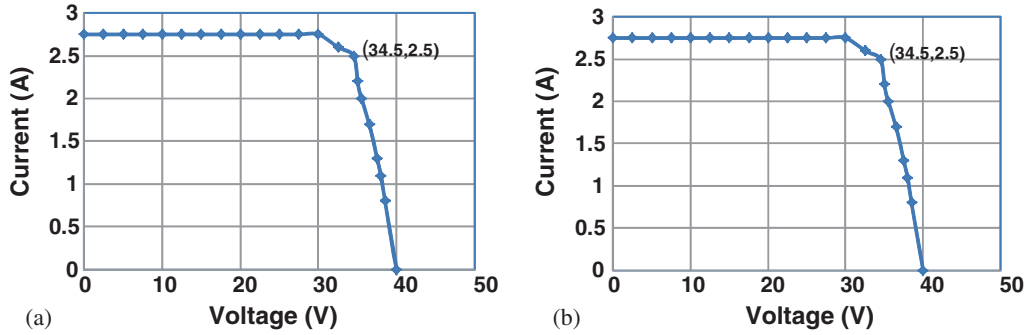


**Figure 15.** (a) current vs. voltage characteristics of PV module; (b) power vs. voltage characteristics of PV module from experimental data.

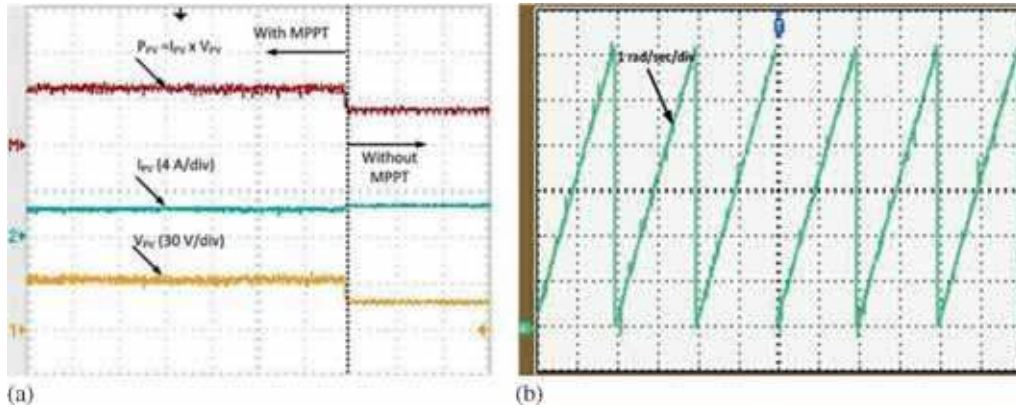


**Figure 16.** (a) Power, current and voltage of PV module with and without MPPT controller; (b) output phase angle of PLL.

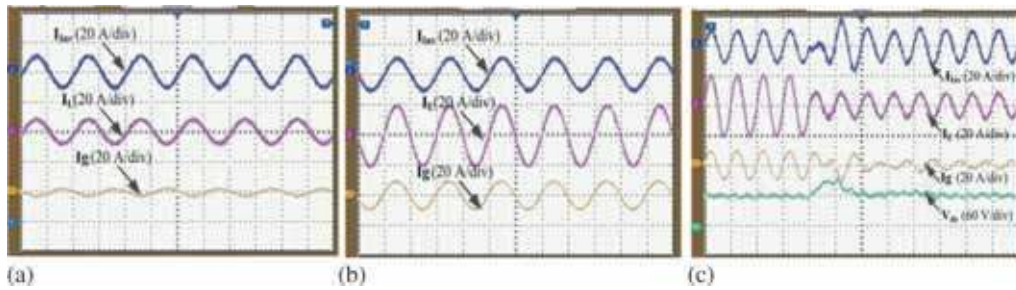


**Figure 17.** Inverter current, load current and grid current under (a) light load or grid feeding condition; (b) overload or load sharing condition; (c) inverter current, load current, grid current and DC-link voltage during transition from overload to light load.

**Table 4.** Comparative analysis of simulated and experimental result during grid connected mode.

	Light load condition			Over load condition		
	$I_{Inv}$	$I_L$	$I_g$	$I_{Inv}$	$I_L$	$I_g$
Simulated results	7.4 A (rms)	5.65A (rms)	1.75 A (rms)	7.4A (rms)	14.14A (rms)	6.74A (rms)
Experimental results	7.59 A (rms)	5.89A (rms)	1.75 A (rms)	7.59 A (rms)	14.38A (rms)	6.80 A (rms)

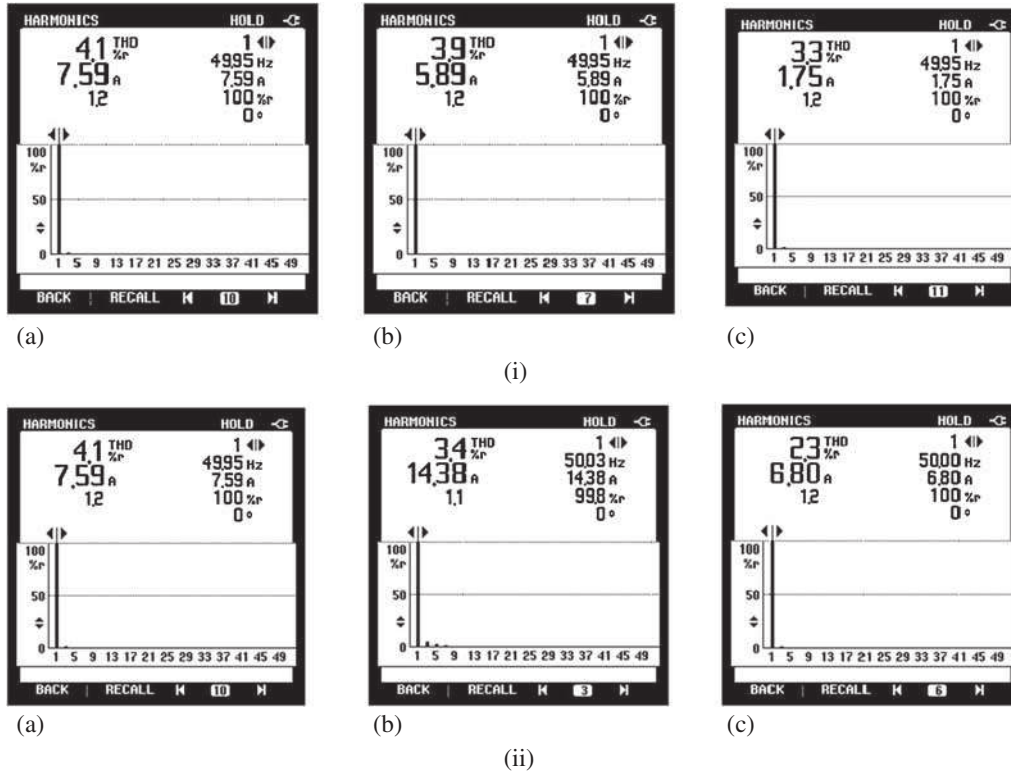


**Figure 18.** Harmonic spectrum of (a) inverter current; (b) load current; (c) grid current under: (i) light load; (ii) overload condition.

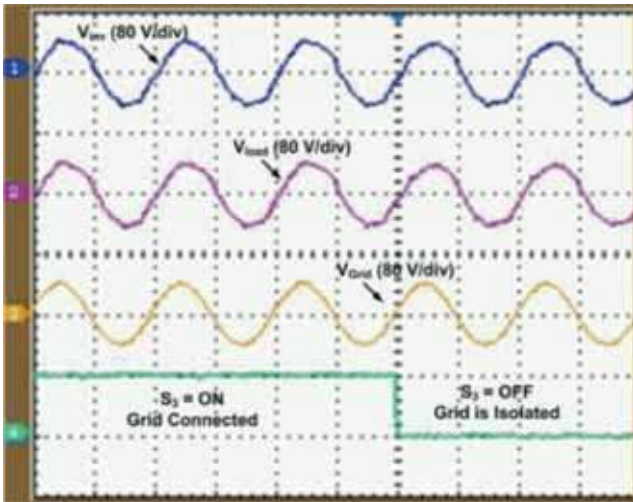


**Figure 19.** Inverter voltage, load voltage and grid voltage under grid connected and isolated grid operation.

table 4. From this table, it is found that simulation results are in good agreement with experimental results.

#### Mode 2: Grid isolation mode

For the testing of prototype model under this mode, a 20  $\Omega$  resistive load is connected across the PV inverter. The inverter voltage, load voltage and grid voltage of the

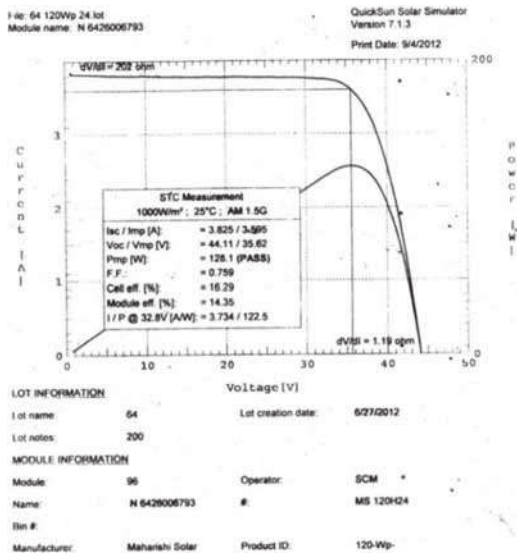
proposed system under this mode are shown in figure 17. The prototype is first operated in grid connected mode and after some instant; the switch between PCC and grid is opened to run the system under isolated grid mode. It is observed from the experimental result in figure that with the voltage control schemes the inverter and load terminal voltage is remained constant even in isolated condition (figure 19).

## 7. Conclusion

This paper has presented a complete control strategy for a single-phase PV inverter operating in both grid connected and grid isolated mode. For the synchronization of PV inverter with the grid a single phase DTDPLL controller is presented. The performance of proposed DTDPLL controller is validated under varying frequency conditions. The grid connected PV system is tested under two different modes of operations, which are PV inverter control during grid connected operation and grid isolation operation. During grid connected operation, PV inverter operates in a current controlled mode. Under this mode of operation, the PV inverter feeds the surplus power to the grid during light load condition, whereas during overload conditions both the PV inverter and grid share the load requirement. During isolated grid operation, the PV inverter operates in voltage-controlled mode to maintain a constant voltage. For the

optimum use of PV module, a modified P&O based MPPT controller has been used. Two 120W PV modules have been used for the prototype development which is interfaced with 40V (peak), 50 Hz single phase grid through a PV inverter. Finally, the developed prototype is tested under all different conditions and is shown to work satisfactorily.

## Appendix A. Datasheet of PV module.



## Nomenclature

$a$	diode ideality constant
$I_0$	reverse saturation current
$i_g$	grid current
$i_{inv}$	inverter output current
$i_L$	load current
$I_{MPP}$	current at the MPP
$I_{PV}$	PV current
$I_{SC}$	short circuit current
$I_{SC,STC}$	nominal short-circuit current
$K$	Boltzmann constant, $1.3806503 \times 10^{-23}$ J/K
$K_I$	short circuit current/temperature coefficient
$K_V$	open circuit voltage/temperature coefficient
$N_s$	number of PV cell in series
$P_{MAX,e}$	maximum experimental peak output power
$Q$	electron charge, $1.60217646 \times 10^{-19}$ C
$R_s$	series resistance
$R_{Sh}$	shunt resistance
$T$	temperature in Kelvin
$v_g$	grid voltage
$V_{MPP}$	voltage at the MPP
$V_{OC}$	open-circuit voltage
$V_{OC,STC}$	nominal open circuit voltage
$V_t$	thermal voltage of PV module

## References

- [1] Blaabjerg F, Teodorescu R, Liserre M and Timbus A V 2006 Overview of control and grid synchronization for distributed power generation systems. *IEEE Trans. Ind. Electron.* 53(3): 1398–1409
- [2] Blaabjerg F, Zhe C and Kjaer S B 2004 Power electronics as efficient interface in dispersed power generation systems. *IEEE Trans. Power Electron.* 19(3): 1184–1194
- [3] Serban E and Serban H 2010 A control strategy for a distributed power generation microgrid application with voltage- and current-controlled source converter. *IEEE Trans. Power Electron.* 25(12): 2981–2992
- [4] Chatterjee A, Keyhani A and Kapoor D 2011 Identification of photovoltaic source models. *IEEE Trans. Energy Convers.* 26(3): 883–889
- [5] Villalva M G, Gazoli J R and Filho E R 2009 Comprehensive approach to modeling and simulation of photovoltaic arrays. *IEEE Trans. Power Electron.* 24(3): 1198–1208
- [6] de Brito M A G, Galotto L, Sampaio L P, de Azevedo e Melo G and Canesin C A 2013 Evaluation of the main MPPT techniques for photovoltaic applications. *IEEE Trans. Ind. Electron.* 60(3): 1156–1167
- [7] Jain S and Agarwal V 2007 Comparison of the performance of maximum power point tracking schemes applied to single-stage grid-connected photovoltaic systems. *IET Electr. Power Appl.* 1(3): 753–762
- [8] Esram T and Chapman P L 2007 Comparison of photovoltaic array maximum power point tracking techniques. *IEEE Trans. Energy Convers.* 22(2): 439–449, doi: 10.1109/tec.2006.874230
- [9] Kjaer S B 2012 Evaluation of the “Hill Climbing” and the “Incremental Conductance” maximum power point trackers for photovoltaic power systems. *IEEE Trans. Energy Convers.* 27(4): 922–929
- [10] Masoum M A, Dehbonei H and Fuchs E F 2002 Theoretical and experimental analyses of photovoltaic systems with voltage- and current-based maximum power-point tracking. *IEEE Trans. Energy Convers.* 17(4): 514–522
- [11] Alajmi B N, Ahmed K H, Finney S J and Williams B W 2011 Fuzzy-logic-control approach of a modified hill-climbing method for maximum power point in microgrid standalone photovoltaic system. *IEEE Trans. Power Electron.* 26(4): 1022–1030
- [12] Rai A K, Kaushika N, Singh B and Agarwal N 2011 Simulation model of ANN based maximum power point tracking controller for solar PV system. *Sol. Energy Mater. Sol. Cells* 95(2): 773–778
- [13] Abdelsalam A K, Massoud A M, Ahmed S and Enjeti P 2011 High-performance adaptive perturb and observe MPPT technique for photovoltaic-based microgrids. *IEEE Trans. Power Electron.* 26(4): 1010–1021
- [14] Munir S and Yun Wei L 2013 Residential distribution system harmonic compensation using PV interfacing inverter. *IEEE Trans. Smart Grid* 4(2): 816–827
- [15] Yi Fei W and Yun Wei L 2013 A grid fundamental and harmonic component detection method for single-phase systems. *IEEE Trans. Power Electron.* 28(3): 2204–2213, <http://www.analog.com/en/search.html?q=ad202jy>, <http://www.telcon.co.uk/PDF%20Files/HTP25.pdf>, <http://www.st.com/web/en/resource/technical/document/datasheet/CD00001584.pdf>

- [16] Busada C, Goxmez Jorge S, Leon A E and Solsona J 2012 Phase-locked loop-less current controller for grid-connected photovoltaic systems. *IET Renew. Power Generation* 6(6): 400–407
- [17] Feola L, Langella R and Testa A 2013 On the effects of unbalances, harmonics and interharmonics on PLL systems. *IEEE Trans. Instrum. Measur.* 62(5): 2399–2409
- [18] Guan-Chyun H and Hung J C 1996 Phase-locked loop techniques. A survey. *IEEE Trans. Ind. Electron.* 43(6): 609–615, <http://www.maharishisolar.com/>
- [19] Monfared M, Sanatkar M and Golestan S 2012 Direct active and reactive power control of single-phase grid-tie converters. *Power Electron. IET* 5(4): 1544–1550
- [20] Thacker T, Boroyevich D, Burgos R and Wang F 2011 Phase-locked loop noise reduction via phase detector implementation for single-phase systems. *IEEE Trans. Ind. Electron.* 58(6): 2482–2490
- [21] Wang Y F and Li Y W 2011 Grid synchronization PLL based on cascaded delayed signal cancellation. *IEEE Trans. Power Electron.* 26(7): 1987–1997
- [22] Carugati I, Donato P, Maestri S, Carrica D and Benedetti M 2012 Frequency adaptive PLL for polluted single-phase grids. *IEEE Trans. Power Electron.* 27(3): 2396–2404
- [23] Golestan S, Monfared M, Freijedo F D and Guerrero J M 2013 Dynamics assessment of advanced single-phase PLL structures. *IEEE Trans. Ind. Electron.* 60(6): 2167–2177
- [24] Simon D and El-Sherief H 1995 Fuzzy logic for digital phase-locked loop filter design. *IEEE Trans. Fuzzy Syst.* 3(2): 211–218
- [25] Colak I and Kabalci E 2013 Implementation of energy-efficient inverter for renewable energy sources. *Electr. Power Components Syst.* 41(1): 31–46
- [26] Jiang Y, Gao F and Pan J 2010 Single-phase phase-shift full-bridge photovoltaic inverter with integrated magnetics. *Electr. Power Components Syst.* 38(7): 832–850
- [27] Orabi M, Ahmed M and Abdel-Rahim O 2013 A single-stage high boosting ratio converter for grid-connected photovoltaic systems. *Electr. Power Components Syst.* 41(5): 896–911
- [28] Rahim N A and Selvaraj J 2007 Hysteresis current control and sensorless MPPT for grid-connected photovoltaic systems. Paper presented at the IEEE International Symposium on Industrial Electronics
- [29] Kotsopoulos A, Duarte J and Hendrix M 2001 A predictive control scheme for DC voltage and AC current in grid-connected photovoltaic inverters with minimum DC link capacitance. Paper presented at the The 27th Annual Conference of the IEEE Industrial Electronics Society
- [30] Ahmed S S and Mohsin M 2011 Analytical determination of the control parameters for a large photovoltaic generator embedded in a grid system. *IEEE Trans. Sustain. Energy* 2(2): 122–130
- [31] Agrawal S, Sekhar P C and Mishra S 2013 Control of single-phase grid connected PV power plant for real as well as reactive power feeding. Paper presented at the IEEE International Conference on Control Applications (CCA), 28–30 August 2013
- [32] Sera D, Teodorescu R and Rodriguez P 2007 PV panel model based on datasheet values. Paper presented at the IEEE International Symposium on Industrial Electronics
- [33] Timbus A, Liserre M, Teodorescu R, Rodriguez P and Blaabjerg F 2009 Evaluation of current controllers for distributed power generation systems. *IEEE Trans. Power Electron.* 24(3): 654–664
- [34] Franklin G F, Powell J D and Emami-Naeini A 2006 *Feedback control of dynamics systems*. Prentice Hall Inc
- [35] Sozer Y and Torrey D A 2009 Modeling and control of utility interactive inverters. *IEEE Trans. Power Electron.* 24(11): 2475–2483
- [36] Ashari M, Keerthipala W W L and Nayar C V 2000 A single phase parallelly connected uninterruptible power supply/demand side management system. *IEEE Trans. Energy Convers.* 15(1): 97–102, doi: 10.1109/60.849123